Harmonic Caching for Walk on Spheres - Supplemental

ZIHONG ZHOU, Dartmouth College, USA
EUGENE D'EON, NVIDIA, New Zealand
ROHAN SAWHNEY, NVIDIA, USA
WOJCIECH JAROSZ, Dartmouth College, USA

ACM Reference Format:
Zihong Zhou, Eugene d'Eon, Rohan Sawhney, and Wojciech Jarosz. 2025. Harmonic Caching for Walk on Spheres - Supplemental. *ACM Trans. Graph.* 44, 6, Article 252 (December 2025), 4 pages. https://doi.org/10.1145/3763322

1 Connection between Harmonic Series Expansion and Poisson Integral Formula

Recall the harmonic series expansion of the 2D Laplace equation in polar coordinates:

$$u(r,\theta) = a_0 + 2\sum_{l=1}^{\infty}\left(\frac{r}{R}\right)^l (a_l \cos l\theta + b_l \sin l\theta), \tag{1}$$

where R is the radius of the disk and a_l, b_l are Fourier coefficients of the boundary function $u(R,\theta)$:

$$a_l = \frac{1}{2\pi}\int_0^{2\pi} u(R,\Theta)\cos(l\Theta)\,\mathrm{d}\Theta, \quad l = 0,1,2,\cdots \tag{2a}$$

$$b_l = \frac{1}{2\pi}\int_0^{2\pi} u(R,\Theta)\sin(l\Theta)\,\mathrm{d}\Theta, \quad l = 1,2,\cdots. \tag{2b}$$

Substituting Eq. (2) into Eq. (1) and applying the trigonometric identity $\cos(l\theta)\cos(l\Theta)+\sin(l\theta)\sin(l\Theta) = \cos(l(\theta-\Theta))$ results in:

$$\frac{1}{2\pi}\left(\int_0^{2\pi} u(R,\Theta)\,\mathrm{d}\Theta + 2\sum_{l=1}^{\infty}\left(\frac{r}{R}\right)^l \int_0^{2\pi} u(R,\Theta)\cos(l(\theta-\Theta))\,\mathrm{d}\Theta\right). \tag{3}$$

Swapping the order of summation and integration gives us:

$$u(r,\theta) = \frac{1}{2\pi}\int_0^{2\pi} u(R,\Theta)\left(1 + 2\sum_{l=1}^{\infty}\left(\frac{r}{R}\right)^l \cos((\theta-\Theta)l)\right)\mathrm{d}\Theta. \tag{4}$$

The series has a closed form expression [Gradshteyn and Ryzhik 2007, 1.447.3] when $\frac{r}{R} < 1$ (which we satisfy in our harmonic caching algorithm: we only extrapolate $u(r,\Theta)$ up to $0.9R$) and then we export the Poisson integral formula for a disk with radius R:

$$u(r,\theta) = \int_0^{2\pi} u(R,\Theta)\underbrace{\frac{1}{2\pi}\frac{R^2-r^2}{R^2-2Rr\cos(\theta-\Theta)+r^2}}_{\text{Poisson kernel } P^B(r,\theta;R,\Theta)}\mathrm{d}\Theta. \tag{5}$$

This is also known as the off-centered mean value property: the solution inside the disk is an average of the solution on the spherical boundary $u(R,\Theta)$ weighted by the (off-centered) Poisson kernel $P^B(r,\theta;R,\Theta)$. It also suggests another way to eliminate the bias introduced by the truncation of harmonic series expansion: we could bypass projecting a finite set of Fourier coefficients and instead, we directly form a Monte Carlo estimate of $u(r,\theta)$ within the ball by correlating solutions at $u(R,\Theta)$:

$$\widehat{u}(r,\theta) = \frac{1}{N}\sum_{j=1}^{N}\frac{\widehat{u}(R,\Theta_j)\,P^B(r,\theta;R,\Theta_j)}{p(\Theta_j)}, \tag{6}$$

where $p(\Theta_i) = \frac{1}{2\pi}$ is the uniform PDF of sampling an angle in 2D. This is also the core idea behind the unpublished concurrent work by Czekanski et al. [2024], though they yet to form a practical caching algorithm and only consider the case of 2D Laplace equation with Dirichlet BC. Shipping this estimator with our harmonic caching algorithm (hence termed *Poisson kernel caching*) enables a more practical variance reduction scheme for WoS. Compared to the harmonic caching algorithm in the main paper, the difference lies in the cache record storage and reconstruction, which we discussed in following sections.

2 Comparing Poisson Kernel Caching with Harmonic Caching

We define:

(1) *Harmonic Caching* to refer our caching algorithm using harmonic series expansion in the main paper. Unless explicitly stated, this algorithm does not use Russian Roulette and simply truncates the series at harmonic truncation order L.
(2) *Poisson Kernel Caching* to refer our caching algorithm using Poisson integral formula in Eq. (5).

2.1 Cache Record Storage

Both of the caching method requires storing a set of cache records:

Harmonic Cache Record. Harmonic caching stores the harmonic cache record, which is a set of Fourier coefficients a_l, b_l in 2D. This is very compact since we use the truncation order $L = 10$ in practice, which is $2L+1$ number of coefficients. When Russian Roulette applied to the unbiased reconstruction, this is a variable set of coefficients but on average we could choose the mean to be $\langle L\rangle = 10$ using a prefix-sum estimator with a geometric distribution [Misso et al. 2022].

Poisson Kernel Cache Record. Poisson kernel caching stores the Poisson kernel cache record, keeping the list of sampled directions $\Theta_1, \cdots, \Theta_N$ along with the WoS estimates $\widehat{u}(R,\Theta_j)$ at each Θ_j. Note that this can be memory intensive since $N \ll L$.

Additional Data in the Record. In addition, each cache record in harmonic or Poisson kernel cache also keeps track of the cache record center's position $\mathbf{p}$, maximum reconstruction radius $R =$

Authors' Contact Information: Zihong Zhou, zihong.zhou.sr.gr@dartmouth.edu, Dartmouth College, USA; Eugene d'Eon, NVIDIA, New Zealand, edeon@nvidia.com; Rohan Sawhney, NVIDIA, USA, rsawhney@nvidia.com; Wojciech Jarosz, Dartmouth College, USA, wojciech.k.jarosz@dartmouth.edu.

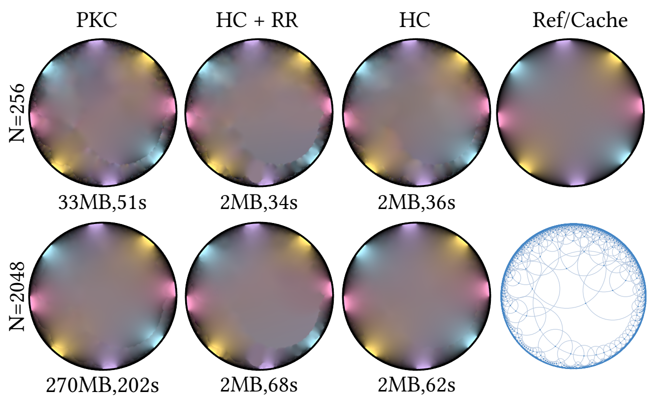

Fig. 1. We compare Poisson kernel caching (PKC), harmonic caching with series truncation (HC), harmonic caching with Russian Roulette (HC + RR) at equal number of cache records with the same reconstruction radius ($0.9R_d$) and same number of walks per cache record ($N = 256$ for top row and $N = 2048$ for bottom row). Both HC+RR and PKC could provide unbiased reconstruction at comparable quality. However, PKC exhibits stronger singularity artifacts and requires much higher storage for the cache. HC provides a higher quality reconstruction at the cost of truncation bias.

$0.9R_d$ where R_d is the closest distance to the domain boundary $\partial\Omega$ and the additional data described in following paragraphs.

2.2 Reconstruction Complexity Analysis

Here we compare the time complexity of reconstructing the solution within a single disk. Recall our Monte Carlo estimator used by harmonic caching with harmonic truncation order L is defined as:

$$\langle \tilde{u}(r,\theta)\rangle := \frac{1}{2}\widehat{a_0} + \sum_{l=1}^{L}\left(\frac{r}{R}\right)^l (\widehat{a_l}\cos l\theta + \widehat{b_l}\sin l\theta). \tag{7}$$

Let C denote the number of Fourier coefficients ($C = 2L + 1$), P the number of evaluation points within the disk, and N the number of boundary samples on the ball. The time complexity for harmonic series reconstruction is:

$$O(\text{Harmonic Series}) = (N \times C + P \times C), \tag{8}$$

while the time complexity for Poisson kernel reconstruction is:

$$O(\text{Poisson Kernel}) = (N \times P). \tag{9}$$

In typical cases, $C \ll B \ll P$: more samples are required to reduce the variance of Fourier coefficients estimation in Eq. (2), or Poisson integral formula estimation in Eq. (5).

In Fig. 1, we show that the Poisson kernel caching can be $2 \sim 3\times$ slower than harmonic caching algorithms (with or without roulette) while $10 \sim 100\times$ more storage than the harmonic caching algorithm in practice (depending on N). As an equal time comparison between PKC and HC+RR, HC+RR can allocate much more cache records to obtain a higher quality reconstruction across the domain as shown in Fig. 2. This suggests that our harmonic caching algorithm (with or without roulette) is preferred over Poisson kernel caching. Unless strict unbiasedness of the series reconstruction is required, harmonic caching without roulette should be the default choice - which is the approach we adopt in our paper.

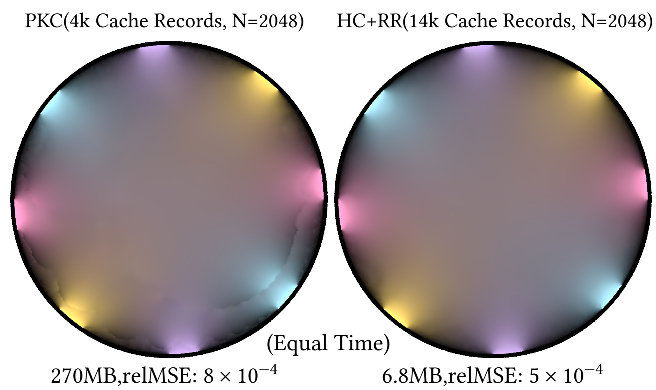

Fig. 2. To perform an equal time comparison for PKC and HC+RR, we simply increase the number of cache records (by increasing w_{sum} from 0 to 1.5) while keeping other parameters unchanged. The storage cost slightly increases but is still negligible compared to PKC and now our HC+RR algorithm has much fewer correlation artifacts with a lower error.

3 Connection between Poisson Kernel Caching and Boundary Value Caching

The boundary value caching method is based on the boundary integral equation [Miller et al. 2023]:

$$u(x) = \underbrace{\int_{\partial\Omega} P^{\mathbb{R}^d}(x,z)\,u(z) \;+\; G^{\mathbb{R}^d}(x,z)\,\frac{\partial u(z)}{\partial n_z}\mathrm{d}z}_{=:u_{\partial\Omega}(x)} + \underbrace{\int_{\Omega} G^{\mathbb{R}^d}(x,y)\,f(y)\mathrm{d}y}_{=:u_{\Omega}(x)}, \tag{10}$$

where $P^{\mathbb{R}^d}, G^{\mathbb{R}^d}$ are free space Poisson kernel and Green's function, respectively and x is within the domain. BVC can be applied to a virtual boundary inside and intersecting the domain Miller et al. [2023, Sec 3.2]. In the case of a virtual sphere fully contained within the domain, we could instead use the Poisson kernel $P^B(x,z)$ and the Green's function of the ball $G^B(x,y)$ centered at x. Then the Green's function $G^B(x,z) = 0$ for $z \in \partial B(x)$ eliminates the second term in the first integral (Eq. (10)):

$$u(x) = \int_{\partial B(x)} P^B(x,z)u(z)\,\mathrm{d}z + \int_{B(x)} G^B(x,y)f(y)\,\mathrm{d}y. \tag{11}$$

This recovers the off-centered mean value property used by Poisson kernel caching. Note that the Poisson kernel is singular at $x = z$ ($r = R$ in Eq. (5)), so both the BVC and PKC are prone to singularity issues.

4 Efficiency Analysis

In this section we describe the details of various two-dimensional experiments that we ran to compare the efficiency of harmonic reconstruction to that of traditional point-wise WoS. Our setup is shown in Figure 3. Both algorithms are used to estimate the solution $u(x)$ for all grid points within a unit square that satisfy $|x| < 0.9$ (Figure 3 (left)). To form roughly equal-time comparisons, the same number of walks is used for each run, either from interior grid points (WoS) or uniformly spaced around the unit sphere (for harmonic

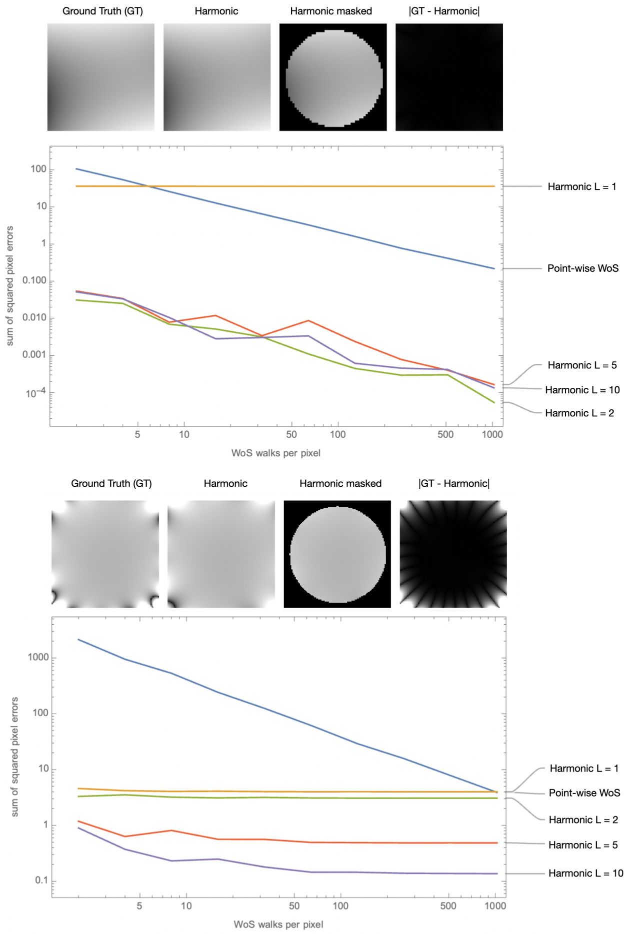

Fig. 4. Top: With a band-limited $L_{GT} = 2$ solution, harmonic reconstruction with too few harmonics ($L = 1$) results in bias that dominates the sum of square errors as the total number of samples per pixel increases, whereas the unbiased WoS method shows the expected $1/n$ behavior predicted by Monte Carlo theory. Because harmonic reconstructions with $L \geq 2$ have no bias for this problem, they also show the same error falloff, but with orders of magnitude lower error than point-wise WoS. Bottom: as the harmonic content of the target solution increases $L_{GT} = 10$, all four harmonic reconstructions applied here eventually exhibit bias that dominates error. At this resolution, however, all harmonic reconstructions exhibit substantially lower total error across the sample rates shown.

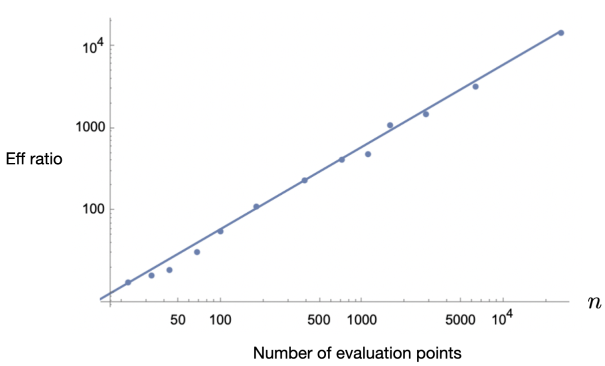

Fig. 5. We observed a linear increase in efficiency of unbiased harmonic reconstruction of a band-limited target ($L_{GT} = L = 10$) compared to point-wise WoS as a function of total reconstruction points n (by varying the grid resolution inside the domain). This shows that harmonic reconstruction can out-perform point-wise WoS by an unbounded margin, provided the query resolution is increased sufficiently.

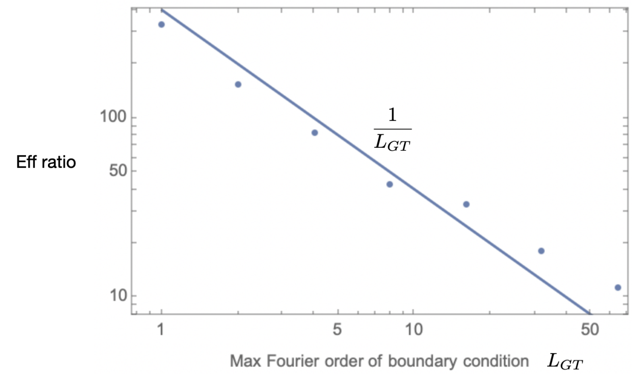

Fig. 6. When comparing the efficiency ratio of harmonic to point-wise WoS, we observed an inverted linear ($1/L_{GT}$) trend as the harmonic order of the ground-truth signal was increased.

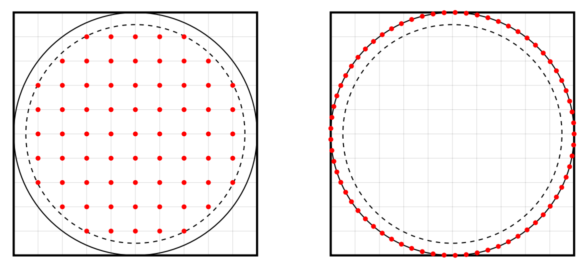

Fig. 3. To compare the efficiency of traditional walk on spheres to our harmonic reconstruction approach, we estimate the solution of a PDE inside a unit square domain in one of two ways. We estimate the solution u at each red point shown in the left figure (for each grid point with a radius $r < 0.9$). For WoS, one walk is spawned from each red point to estimate the solution there. To form an equal-time comparison for our harmonic approach, we spawn the same number of walks as in the left configuration, but now placed uniformly around the unit circle (right). These are then used to reconstruct the interior solution at each of the grid locations inside the radius 0.9 circle (i.e. the same positions as shown on the left).

reconstruction). In the latter case, after estimating harmonic coefficients, the solution is reconstructed in the interior at the same grid points that WoS computed directly, and the sum of squared errors is computed relative to the ground truth.

For each experiment, we prescribed an analytic ground truth solution over the entire domain by generating a random, truncated harmonic representation extended over the full square. The values of this solution at the boundary of the square were used as the Dirichlet boundary condition. We varied the grid (pixel) resolution for evaluation points (which changed the number of reconstruction points n), the screening parameter α, the harmonic truncation order L, the maximum harmonic order of the ground truth function L_{GT} and the number of walks per evaluation point (pixel).

Figure 4 (top) illustrates that the harmonic approach exhibits the expected $1/n$ error rate of traditional point-wise Monte Carlo, provided the truncation order L is higher than that of the reconstructed ground truth signal. And as the harmonic order of the target increases (bottom), the error curves clearly show how bias dominates eventually.

References

Michael Czekanski, Benjamin Faber, Margaret Fairborn, Adelle Wright, and David Bindel. 2024. Walking on Spheres and Talking to Neighbors: Variance Reduction for Laplace's Equation. arXiv:physics/2404.17692

I. S. Gradshteyn and I. M. Ryzhik. 2007. *Table of Integrals, Series, and Products* (7 ed.). Academic Press.

Bailey Miller, Rohan Sawhney, Keenan Crane, and Ioannis Gkioulekas. 2023. Boundary Value Caching for Walk on Spheres. *ACM Transactions on Graphics (Proceedings of SIGGRAPH)* 42, 4 (July 2023), 82:1–82:11. https://doi.org/10/gsk4f8

Zackary Misso, Benedikt Bitterli, Iliyan Georgiev, and Wojciech Jarosz. 2022. Unbiased and Consistent Rendering Using Biased Estimators. *ACM Transactions on Graphics (Proceedings of SIGGRAPH)* 41, 4 (July 2022), 48:1–48:13. https://doi.org/10/gqjn66